COMPDYN 2013
4th ECCOMAS Thematic Conference on
Computational Methods in Structural Dynamics and Earthquake Engineering
M. Papadrakakis, V. Papadopoulos, V. Plevris (eds.)
Kos Island, Greece, 12–14 June 2013

IDENTIFYING THE DAMPING CONTRIBUTION OF BUILDING COMPONENTS BASED ON MEASURED TOP VIBRATION

Ronald L.J. van den Berg[1*], Raphaël D.J.M. Steenbergen[1],

[1] TNO Built Environment and geosciences, PO Box 49, NL 2600 AA Delft, The Netherlands
e-mail: rlj.vandenberg@tno.nl, raphael.steenbergen@tno.nl

Keywords: wind, dynamics, damping, tall buildings, comfort.

Abstract. *In this paper, a damping model for a high-rise building is introduced. This model is used to investigate the possibilities to identify the relative damping contribution of the internal material damping in building elements, energy loss at element interfaces and energy outflow at the interface with the ground. The building is modeled as an Euler-Bernoulli beam which is elastically supported at its base by a translational and rotation spring, including viscous damping elements. The beam has internal viscous material damping and is attached to a distributed viscous damper. Data obtained from conventional full scale measurements of the vibrations at the top of a high-rise building, is used to calibrate the model. Values of the model parameters which result in a best fit, are found from calculation of the least square error between the simulated and measured response. It is concluded that the conventional performed measurements don't provide enough data to uniquely determine the relative contribution of the different damping components. A new measurement method is needed in order to identify the relative contribution.*

1 INTRODUCTION

The design of Dutch high-rise buildings is dominated by the effect of dynamic wind loads. A minimum stiffness is required to keep the maximum occurring deflection during the lifetime of a building below the maximum allowable deformation. In most cases this aspect is leading in the design process. The dynamic wind load will also introduce vibrations of the building. Especially slender high-rise buildings are sensitive to these vibrations, because their natural frequencies (typically between 0.1-0.5 Hz) correspond with the low frequency region, in which the strongest wind gusts appear, causing a resonance effect. Vibrations with large accelerations can be noticeable for occupants. To avoid uncomfortable situations the maximum occurring accelerations should be lower than restrictions given in ISO6897 [1]. The application of high strength building materials and new building techniques, makes it possible to construct more slender and lighter high-rise buildings that satisfy the deflection criterion. However these high-rise buildings are more sensitive to the wind-induced vibrations and consequently the comfort criteria becomes more governing in the design. Dutch high-rise buildings are relatively slender in comparison with foreign buildings, because of the stern

legislation on daylight entrance. As a result of this comfort and legislation issues, the building height of Dutch residential buildings appears nowadays to be limited to about 160 m.

The dynamic response of a tall building depends on its mass, stiffness and damping properties. The maximum occurring acceleration depends to a large extend on the damping properties, while in contrast with the mass and stiffness, it is difficult to accurately estimate the damping because of its complex physical nature. The total energy dissipation in a building is a combination of the internal material damping in building elements, energy loss at element interfaces and energy outflow at the interface with the ground (soil structure interaction, see Figure 1). At this point the aerodynamic damping is neglected for tall buildings [2].

Structural designers, normally use the damping ratios that are based on measurement of actual building vibrations. The total damping of the primary vibration modes of a building are determined from measurement of the vibrations in *x*, *y* and torsion direction at the top floor, during strong winds. Damping ratios are indicated in the annex of Eurocode 1991-1-4 [3], 0.8% and 1.6% for steel and reinforced concrete structures respectively. However actual damping ratios of Dutch buildings deviate a lot from these values. Ratios up to 2-3% for steel structures and minimum values of 1.0% for reinforced concrete structures have been observed [4]. This illustrates the uncertainty around the used damping values.

Based on the observed damping behavior of reinforced concrete buildings, Jeary [5] explained the structural damping is caused by friction forces at interfaces between structural members and in microcracks inside the material. Based on this mechanism, an empirical formula with a low amplitude plateau, related to the frequency, is deduced. Also an increasing damping for increasing amplitude is deduced. Lagomarsino [6] performed statistical analyses on the damping ratios of 185 buildings to establish an empirical relation between the damping value in the low amplitude region and the natural frequency. Relations have been found for reinforced concrete, steel and mixed structures. It is also claimed that the internal material damping for steel structures is negligible in comparison with the damping at element interfaces. Furthermore some particular interesting results considering the amount of partition walls are indicated. Most recently Satake et. al. [7] studied the damping properties of 205 Japanese buildings and obtain an empirical formula based on Jeary's mechanism.

Despite these empirical formulae which are based on results for multiple buildings, their results show a lot of scatter because there is a large variety of buildings and relatively few buildings have been measured. The amplitude dependency makes it even more difficult to make a good comparison between different damping ratios.

By monitoring the vibrations of individual buildings over longer periods of time, in-depth investigations to the damping properties of buildings have been performed [8]. In the Chicago Full-Scale Monitoring Program [9], the dynamic response of 3 tall buildings has been monitored over a decade to study the amplitude dependency of the damping. Furthermore higher damping levels are observed at structural systems with a greater degree of frame action than cantilever action.

Up till now, researchers have tried to get a grip on the damping behavior of tall buildings, by studying the overall damping. Since this total damping is a result of many different energy dissipation mechanisms, it is particulary difficult to find a clear relation between this overall damping behavior and the building properties. Therefore it is proposed to focus on a method to identify the damping contribution of different building parts. In this way, their damping behavior with respect to the corresponding building part characteristics can be studied separately.

For this purpose, a dynamic building model is developed in which 4 viscous damping parameters represent the damping in different parts. First an explanation about the assumed mass, stiffness and damping properties in this model is given. The use of the model to identify

the relative damping contribution of building parts is illustrated by comparison of the dynamic behavior of this model with the response data of a real full-scale measurement.

2 BUILDING MODEL

2.1 Set-up of the model, equation of motion and boundary conditions

The dynamic behavior of a high-rise building is analyzed by considering its deflection due to an along-wind loading. Because most tall buildings are symmetrical, the deflection of the centre of rotation can be analyzed as a 2-dimensional problem. The deflection due to rotation can be neglected at this point. A model is developed (see Figure 1) in which a high-rise building is represented by an Euler-Bernoulli beam with distributed mass ρA, elastically supported at its base and subjected to an along-wind load $q(z,t)$.

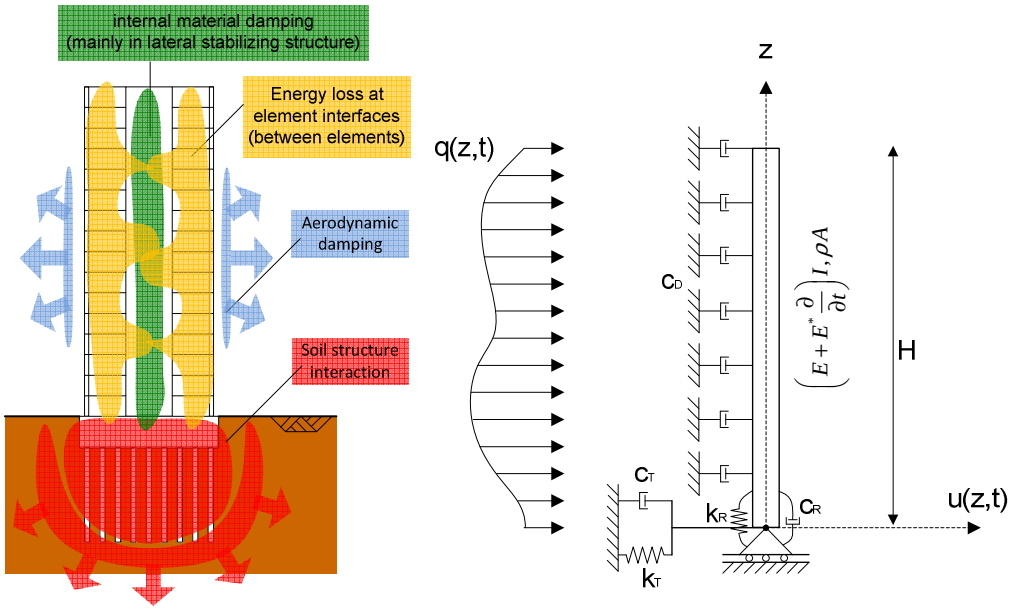

Figure 1 – Damping sources and dynamic model of a high-rise building

Since high-rise buildings are slender, the shear deformation is small in comparison with the bending deformation and can be neglected [10]. In addition the deformations are small compared to the building's dimensions. These two aspects justify the use of the Euler-Bernoulli beam to model the deformation of a high-rise building. The foundation of the building can rotate and translate under a horizontal load. The elastic rotation stiffness of the piles and soil is modeled with a rotational spring (k_R). The reaction of the soil against the translation of the underground structure in horizontal direction is represented by translational spring (k_T). Energy will be lost during loading and unloading of the soil. This damping due to soil-structure interaction is modeled by a translational (c_T) and rotational (c_R) viscous damper.

Internal material damping of a beam can be represented by a viscous damping model which is introduced by adding a time-dependent term to the modulus of elasticity.

$$E^* \frac{\partial}{\partial t} \tag{1}$$

In this way the stresses in the material are modeled according to the Kelvin-Voigt model. The non-structural elements of a building will move relative to each other, or relative to the main load bearing structure. Energy will be lost due to friction at the interfaces between these

elements. This energy loss has been modeled by the distributed dampers (c_D) across the whole length of the beam.

The transverse vibration of the beam is governed by a partial differential equation, the equation of motion (EM), in which *u(z,t)* is the transverse deflection of the beam at position *z* and time *t*.

$$\rho A\frac{\partial^2 u}{\partial t^2}+EI\frac{\partial^4 u}{\partial z^4}+E^*I\frac{\partial^5 u}{\partial t\partial z^4}+c_d\frac{\partial u}{\partial t}=q(z,t) \tag{2}$$

The boundary conditions (BCs) of the system at z=0 and z=H are

$$\left(E+E^*\frac{\partial}{\partial t}\right)I\frac{\partial^2 u}{\partial z^2}\bigg|_{z=0}=k_R\frac{\partial u}{\partial z}\bigg|_{z=0}+c_R\frac{\partial^2 u}{\partial z\partial t}\bigg|_{z=0} \tag{3}$$

$$-\left(E+E^*\frac{\partial}{\partial t}\right)I\frac{\partial^3 u}{\partial z^3}\bigg|_{z=0}=k_T u(0,t)+c_T\frac{\partial u}{\partial t}\bigg|_{z=0} \tag{4}$$

$$\left(E+E^*\frac{\partial}{\partial t}\right)I\frac{\partial^2 u}{\partial z^2}\bigg|_{z=H}=0 \tag{5}$$

$$\left(E+E^*\frac{\partial}{\partial t}\right)I\frac{\partial^3 u}{\partial z^3}\bigg|_{z=H}=0 \tag{6}$$

2.2 Natural frequencies and mode shapes

For low modal damping ratios (ζ<0.10; as observed at the measured tall buildings), the natural frequency and mode shapes can be found by neglecting all damping mechanisms and solve the homogeneous EM.

$$\rho A\frac{\partial^2 u}{\partial t^2}+EI\frac{\partial^4 u}{\partial z^4}=0 \tag{7}$$

The BCs of the system at z=0 and z=H are:

$$EI\frac{\partial^2 u}{\partial z^2}\bigg|_{z=0}=k_R\frac{\partial u}{\partial z}\bigg|_{z=0} \tag{8}$$

$$-EI\frac{\partial^3 u}{\partial z^3}\bigg|_{z=0}=k_T u(0,t) \tag{9}$$

$$EI\frac{\partial^2 u}{\partial z^2}\bigg|_{z=H}=0 \tag{10}$$

$$EI\frac{\partial^3 u}{\partial z^3}\bigg|_{z=H}=0 \tag{11}$$

The solution *u(z,t)* is assumed as the multiplication of an unknown coordinate related function, *U(z)* and an unknown time related function, $\psi(t)$.

$$u(z,t)=U(z)\Psi(t) \tag{12}$$

Using the method of separation of variables by inserting Eq. (12) in (7), the EM can be separated into the time and coordinate related differential equation.

$$\ddot{\Psi}+\omega_n^2\Psi=0 \tag{13}$$

$$U^{IV} - \beta^4 U = 0 \tag{14}$$

where

$$\beta^4 = \frac{\rho A \omega_n^{\,2}}{EI} \tag{15}$$

ω_n is the natural frequency. A dot denotes differentiation with respect to time t and roman numbers indicate differentiation with respect to position z. The time and coordinate related part are standard second and fourth order differential equations and their general solution can easily be derived.

$$\Psi(t) = A\sin(\omega_n \cdot t) + B\cos(\omega_n \cdot t) \tag{16}$$

$$U(z) = C_1\cosh(\beta \cdot z) + C_2\sinh(\beta \cdot z) + C_3\cos(\beta \cdot z) + C_4\sin(\beta \cdot z) \tag{17}$$

Constants A en B depend on the initial conditions and C_1-C_4 depend on the BCs. By substitution of the general solutions into the BCs, a set of 4 algebraic equations is obtained.

$$\underline{\underline{A}}\,\underline{C} = \underline{0} \tag{18}$$

$$EI\beta^2 \begin{bmatrix} 1 & -\frac{k_R}{EI\beta} & -1 & -\frac{k_R}{EI\beta} \\ k_T & \beta & k_T & -\beta \\ \cosh(\beta H) & \sinh(\beta H) & -\cos(\beta H) & -\sin(\beta H) \\ \beta\sinh(\beta H) & \beta\cosh(\beta H) & \beta\sin(\beta H) & -\beta\cos(\beta H) \end{bmatrix} \begin{bmatrix} C_1 \\ C_2 \\ C_3 \\ C_4 \end{bmatrix} = \begin{bmatrix} 0 \\ 0 \\ 0 \\ 0 \end{bmatrix} \tag{19}$$

Constants C_1-C_4 are found by solving this set of algebraic equations. To find the non-trivial solution of the set of equations, the determinant of A has to be equal to zero. The expression of the determinant is a function of ω_n. By setting this expression equal to zero, the frequency equation is obtained. This transcendental equation has infinite amount of solutions, which are the natural frequencies of the system. By substitution of the found natural frequencies in the set of equations, $C_{1,i}$-$C_{4,i}$ can be found for every natural frequency $\omega_{n,i}$. The natural frequencies are defined such that the determinant is zero, consequently the system is dependent. This means that the constants $C_{1,i}$-$C_{4,i}$ that need to be found depend on each other. In order to find the shapes of the modes, it is assumed that $C_{4,i}$=1. The total solution of the undamped free vibration is a summation over all modes. A_i and B_i depend on the initial conditions.

$$\begin{aligned} u(z,t) &= \sum_{i=1}^{\infty} U_i(z)\Psi_i(t) \\ U_i(z) &= C_{1,i}\cosh(\beta_i z) + C_{2,i}\sinh(\beta_i z) + C_{3,i}\cos(\beta_i z) + C_{4,i}\sin(\beta_i z) \\ \Psi_i(t) &= A_i\sin(\omega_{n,i} t) + B_i\cos(\omega_{n,i} t) \\ \beta_i^4 &= \frac{\rho A \omega_{n,i}^{\,2}}{EI} \end{aligned} \tag{20}$$

2.3 Calibation of the mass and stiffness to the measured natural frequency

On the 6th of December 2011, the accelerations at the top of a high-rise building in the centre of Rotterdam were monitored with 6 accelerometers. The accelerometers were placed as indicated in Figure 2. With the response-time data from these devices, it was possible to determine the vibrations in the three main directions of the building (x- and y-translation and

torsion). The data concerning the time-response in *x*-direction is used to illustrate the damping identification.

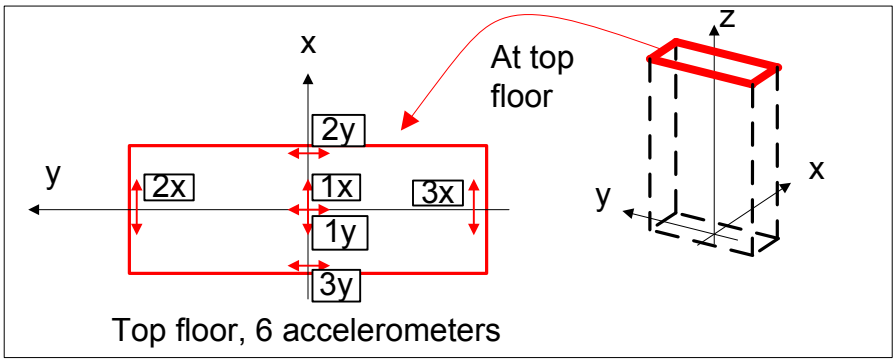

Figure 2 – monitoring of the accelerations with 6 accelerometers at the top of the building

Representative values of the model parameters concerning the mass, stiffness and height are derived from the design calculations of this building. By inserting these values in (19), the corresponding natural frequencies and mode shapes are found. The natural frequency of the first mode in the model is equal to $f_n=\omega_n/2\pi$ =3.39 /2π=0.230 Hz, however it doesn't correspond with the first natural frequency that is measured (f_n=0.536 Hz). Based on a sensitivity analysis and because of the conservative assumptions in the design process, a lower mass and higher stiffness have been assumed in order to calibrate the natural frequency of the model to the measurements [4]. Values of the calibrated mass, stiffness and mode shapes can be found in Table 1, Table 2 and Figure 3.

ρA [kg/m]	EI [Nm^2]	k_R [Nm/rad]	k_T [N/m]	H [m]
$2.30\cdot10^5$	$7.44\cdot10^{13}$	$4.42\cdot10^{12}$	$1.00\cdot10^{11}$	121.5

Table 1 – overview of calibrated mass and stiffness model parameters

Mode	ω [rad/s]	$C_{1,i}$	$C_{2,i}$	$C_{3,i}$	$C_{4,i}$
1	3.43	0.93	-0.57	-0.92	1
2	22.62	0.46	-0.48	-0.41	1

Table 2 –natural frequencies and corresponding mode shape constants for calibrated mass and stiffness

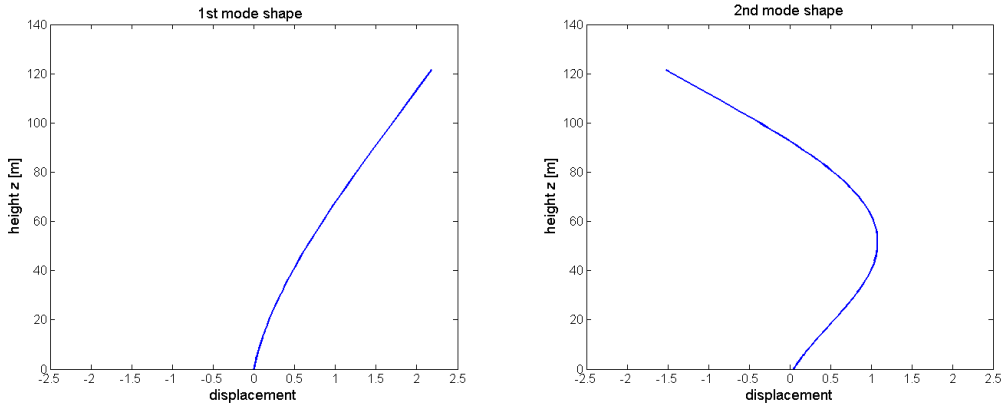

Figure 3 – Mode shapes of the first two translational bending modes

3 SIMULATED DYNAMIC RESPONSE

3.1 Wind loading conditions

No information about the local wind loading conditions were obtained during the monitoring of the response. Therefore theoretically based assumptions about the along-wind load are made to represent the statistical characteristics of the random wind load to which the building was subjected. The along-wind load at height z is split in a mean, $\overline{v}$ and fluctuating part $\tilde{v}$ [11].

$$p_w = \frac{1}{2}\rho_{air} v^2 = \frac{1}{2}\rho_{air}\left(\overline{v}+\tilde{v}\right)^2 = \frac{1}{2}\rho_{air}\left[\overline{v}^2 + 2\cdot\overline{v}\cdot\tilde{v} + \tilde{v}^2\right] \tag{21}$$

Since the fluctuating response was monitored around the mean deflection of the building, only the fluctuating wind load is modeled.

$$\tilde{q}(z,t) = B\cdot C_f \cdot \tilde{p}_w(z,t) = B\cdot C_f \cdot \rho_{air}\cdot\overline{v}(z)\cdot\tilde{v}(z,t) \tag{22}$$

The width B is constant over height. C_f is the shape factor which is inserted as an average of the local shape factors over the frontal area of the building. The term $\tilde{v}^2$ is neglected because it is relatively small. The mean wind velocity is described by a logarithmic wind profile depending on z. Gusts are the fluctuating part of the wind speed in time. A spectral description of the turbulence is a convenient tool to account for the energy contained in the sequence of gusts. The single sided variance spectrum of the fluctuating velocity (S_{vv}), shows how the energy of a sequence of gusts is distributed over the frequencies of the gusts. Because at a certain height there is a linear relation between the fluctuating wind velocity and wind load, the Fourier transform of the fluctuating wind load (S_q) and the single sided variance spectrum of the fluctuating wind load (S_{qq}) are equal to [11]:

$$S_q(z,\omega) = B\cdot C_f\cdot\rho_{air}\cdot\overline{v}_0\ln\left(\frac{z}{z_0}\right)\cdot S_v(z,\omega) \tag{23}$$

$$S_{qq}(z,\omega) = \left[B\cdot C_f\cdot\rho_{air}\cdot\overline{v}_0\ln\left(\frac{z}{z_0}\right)\right]^2 S_{vv}(z,\omega) \tag{24}$$

The shape of the wind spectrum (F_D) as given in the Eurocode [3] has been adopted for the wind velocity spectrum, the total variance (σ_v^2) is unknown. The shape of the spectrum is assumed to be constant over height with $z=z_s=0.6H$. Using the shape (F_D) of the spectrum, the following expression for the load spectrum is derived:

$$S_{qq}(z,\omega) = \left[B\cdot C_f\cdot\rho_{air}\cdot\overline{v}_0\ln\left(\frac{z}{z_0}\right)\right]^2\cdot\frac{\sigma_v^2}{\omega}F_D\left(z=0,6H;\ f=\frac{\omega}{2\pi}\right) \tag{25}$$

On a large surface, the peaks of the wind velocity at different places won't occur at exactly the same time. Thus the total wind load on a larger surface shows less variance. To take this effect into account, the spectrum has to be multiplied with the aerodynamic admittance $\chi(\omega)$.

$$S_{q_e q_e}(z,\omega) = \chi(\omega)^2\left[B\cdot C_f\cdot\rho_{air}\cdot\overline{v}_0\ln\left(\frac{z}{z_0}\right)\right]^2\cdot\frac{\sigma_v^2}{\omega}F_D\left(z=0,6H;\ f=\frac{\omega}{2\pi}\right) \tag{26}$$

In which (for R_b take H=B) [12]

$$\chi(\omega)^2 = R_h R_b \quad [-] \tag{27}$$

$$R_h = \frac{1}{\eta} - \frac{1-e^{-2\eta}}{2\eta^2} \tag{28}$$

$$\eta = \frac{4,6 \cdot \left(\frac{\omega}{2\pi}\right) \cdot H}{\overline{v}(z_s)} \tag{29}$$

The expression for the wind loading spectrum at different heights consists out of a constant part with unknown magnitude, a coordinate related part and a frequency dependent part.

$$S_{q_e q_e}(z,\omega) = C_w \cdot Q_z(z) \cdot Q_{\omega\omega}(\omega) \tag{30}$$

In which

$$\begin{aligned} C_w &= \left[B \cdot C_f \cdot \rho_{air} \cdot \overline{v}_0 \cdot \sigma_v \right]^2 \\ Q_z(z) &= \left[\ln\left(\frac{z}{z_0}\right) \right]^2 \\ Q_{\omega\omega}(\omega) &= \frac{\chi(\omega)^2 F_D\left(z = 0,6H;\ f = \frac{\omega}{2\pi}\right)}{\omega} \end{aligned} \tag{31}$$

3.2 The steady state response

The steady state response is determined from the EM and BCs as given in Eq. (2)-(6). Because the EM contains two terms related to damping (E^* and c_d) and the BCs contain damping terms (c_R and c_T), the equations can't be decoupled by making use of the modal analysis. Therefore the EM and BCs are transformed to the frequency domain by making use of the Fourier transformation:

$$\begin{aligned} &\int_{-\infty}^{\infty} \frac{\partial u(z,t)}{\partial t} \cdot e^{-i\omega t} dt = i\omega \int_{-\infty}^{\infty} u(z,t) \cdot e^{-i\omega t} dt = i\omega \cdot \tilde{U}_F(z,\omega) \\ &\int_{-\infty}^{\infty} \frac{\partial^2 u(z,t)}{\partial t^2} \cdot e^{-i\omega t} dt = i\omega \int_{-\infty}^{\infty} \frac{\partial u(z,t)}{\partial t} \cdot e^{-i\omega t} dt = -\omega^2 \int_{-\infty}^{\infty} u \cdot e^{-i\omega t} dt = -\omega^2 \cdot \tilde{U}_F(z,\omega) \\ &\textit{etc.} \end{aligned} \tag{32}$$

For every ω, the transformed EM is an ordinary differential equation with respect to z.

$$\tilde{U}_F(z,\omega)^{IV} - \beta_F{}^4 \tilde{U}_F(z,\omega) = \frac{\tilde{Q}_F(z,\omega)}{EI + i\omega E^* I} \tag{33}$$

In which

$$\begin{aligned} \beta_F{}^4 &= \frac{\rho A \omega^2 - i\omega c_d}{EI + i\omega E^* I} \\ \tilde{Q}_F(z,\omega) &= \int_{-\infty}^{\infty} q(z,t) \cdot e^{-i\omega t} dt \end{aligned} \tag{34}$$

The BCs, for z=0 become:

$$\left(EI + i\omega E^* I\right)\cdot \tilde{U}_F{}^{II} - k_R \cdot \tilde{U}_F{}^{I} - i\omega c_R \cdot \tilde{U}_F{}^{I} = 0 \tag{35}$$

$$\left(EI + i\omega E^* I\right)\cdot \tilde{U}_F{}^{III} + k_T \tilde{U}_F + i\omega c_T \tilde{U}_F = 0 \tag{36}$$

and for z=H:

$$\left(EI + i\omega E^* I\right)\cdot \tilde{U}_F{}^{II} = 0 \tag{37}$$

$$\left(EI + i\omega E^* I\right)\cdot \tilde{U}_F{}^{III} = 0 \tag{38}$$

Based on the derived wind loading spectrum (30), the Fourier transform of the load consist out of a multiplication of a constant, a logarithmic z-dependent function and a part depending on ω. To simplify calculations, the logarithmic function is fitted by an exponential functional.

$$\tilde{Q}_F(z,\omega) = \sqrt{C_w} Q_\omega(\omega) \ln\left(\frac{z}{z_0}\right) \rightarrow \sqrt{C_w} Q_\omega(\omega)\left(b_2 + b_1 \cdot e^{-z/c}\right) \tag{39}$$

The general solution of Eq. (33) to a load as in (39) $\left(\sqrt{C_w} = 1\right)$ is equal to:

$$\begin{aligned}
\tilde{U}_F(z,\omega) &= \tilde{C}_1 \cosh(\beta_F z) + \tilde{C}_2 \sinh(\beta_F z) + \tilde{C}_3 \cos(\beta_F z) + \tilde{C}_4 \sin(\beta_F z) \\
&\quad + C_0(\omega) + C_z(\omega) e^{-z/c} \\
C_0(\omega) &= \frac{-b_2 Q_\omega(\omega)}{\beta^4\left(EI + i\omega E^* I\right)} \\
C_z(\omega) &= \frac{b_1 Q_\omega(\omega)}{EI + i\omega E^* I} \frac{1}{\left[\left(-\frac{1}{c}\right)^4 - \beta^4\right]}
\end{aligned} \tag{40}$$

For every ω, the constants can be calculated from the 4 algebraic equations that can be found by substitution of the general solution into the BCs:

$$\left(EI + i\omega E^* I\right)\beta_F{}^2 \begin{bmatrix} 1 & -\frac{k_R + i\omega c_R}{\left(EI + i\omega E^* I\right)\beta_F} & -1 & -\frac{k_R + i\omega c_R}{\left(EI + i\omega E^* I\right)\beta_F} \\ \frac{k_T + i\omega c_T}{\left(EI + i\omega E^* I\right)\beta_F{}^2} & \beta_F & \frac{(k_T + i\omega c_T)}{\left(EI + i\omega E^* I\right)\beta_F{}^2} & -\beta_F \\ \cosh(\beta_F H) & \sinh(\beta_F H) & -\cos(\beta_F H) & -\sin(\beta_F H) \\ \beta \sinh(\beta_F H) & \beta \cosh(\beta_F H) & \beta \sin(\beta_F H) & -\beta \cos(\beta_F H) \end{bmatrix} \begin{bmatrix} \tilde{C}_1 \\ \tilde{C}_2 \\ \tilde{C}_3 \\ \tilde{C}_4 \end{bmatrix} = \begin{bmatrix} F_{0,1} \\ F_{0,2} \\ F_{0,3} \\ F_{0,4} \end{bmatrix} \tag{41}$$

In which

$$
\begin{aligned}
F_{0,1} &= -\left[\left(EI + i\omega E^{*}I\right)\cdot\left(-\frac{1}{c}\right)^{2} + k_R \cdot \frac{-1}{c} + i\omega c_R \cdot \frac{-1}{c}\right] C_z(\omega) \\
F_{0,2} &= -\left[\left(EI + i\omega E^{*}I\right)\cdot\left(-\frac{1}{c}\right)^{3} - k_T - i\omega c_T\right] C_z(\omega) - \left[k_T + i\omega c_T\right] C_0(\omega) \\
F_{0,3} &= -\left(EI + i\omega E^{*}I\right)\cdot\left(-\frac{1}{c}\right)^{2} C_z(\omega) e^{-H/c} \\
F_{0,4} &= -\left(EI + i\omega E^{*}I\right)\cdot\left(-\frac{1}{c}\right)^{3} C_z(\omega) e^{-H/c}
\end{aligned}
\tag{42}
$$

From (40)-(42) a linear relation between the load (Q_ω) and the response (U_F) can be observed. The velocity response is obtained by multiplication of the response with $i\omega$. The transfer function (see Figure 4) for the velocity at the top, H_{vTop} ,is the response to a unit load $Q_\omega(\omega)=1$.

$$H_{vTop}(\omega) = i\omega \cdot \tilde{U}_F\left(H, \omega, Q_\omega(\omega) = 1\right) \tag{43}$$

Because of the linear relation, in accordance with (23), (24) and (31), the single sided variance spectrum of the velocity at the top is equal to:

$$S_{vvTopP} = \left|H_{vTop}(\omega)\right|^2 C_w Q_{\omega\omega}(\omega) \tag{44}$$

In which

$$C_w Q_{\omega\omega}(\omega) = \left[B \cdot C_f \cdot \rho_{air} \cdot \bar{v}_0 \cdot \sigma_v\right]^2 \chi(\omega)^2 \frac{F_D\left(z = 0,6h;\, f = \dfrac{\omega}{2\pi}\right)}{\omega} \tag{45}$$

The right hand side of (44) doesn't contain the logarithmic distribution anymore because this is incorporated in the transfer function.

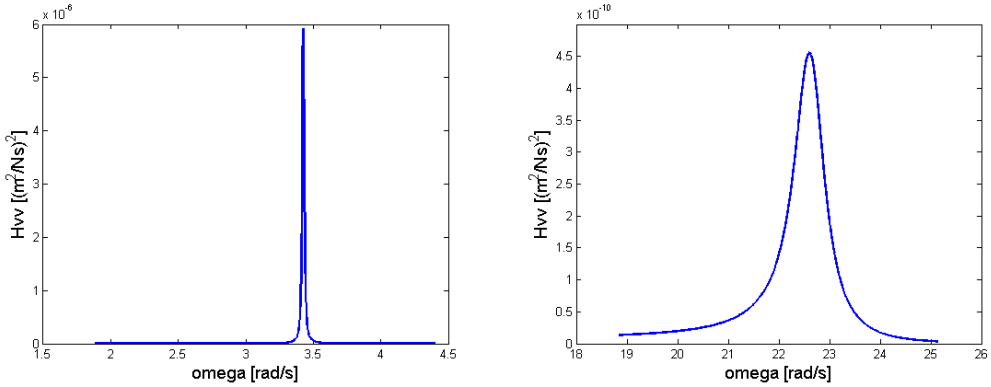

Figure 4 – Transfer function at the first and second natural frequency

4 CALIBRATION OF THE MODEL

4.1 Measured spectrum

The single sided variance spectrum of the time response signal in the main translation *x*-direction is obtained using Welch's method [13]. In this method, the measured signal is divided in multiple segments that partly overlap (50%). The spectrum of each segment is obtained

by using the Fast Fourier Transform (FFT). These spectra are averaged to find the spectrum of the complete time signal. Because of averaging, this method results in a smoother spectrum than by application of the FFT on the complete signal.

The response has been measured for 2 hours during a typical autumn storm (maximum 1-hour-average wind speed of 12 m/s and a maximum peak wind speed of 22 m/s) with a sampling frequency (f_s) of 50 Hz (360448 data points). Because averaging the signal with more segments will decrease the resolution of the spectrum, it has been decided to subdivide the signal in 10 segments, leading to a resolution of 0.0048 rad/s. From the definition of the single sided response spectrum [11], the area under the single sided variance spectrum is equal to the variance (σ_v^2). To check the statistical properties of the spectrum, the area has been compared to the standard deviation of the time signal (see Figure 5).

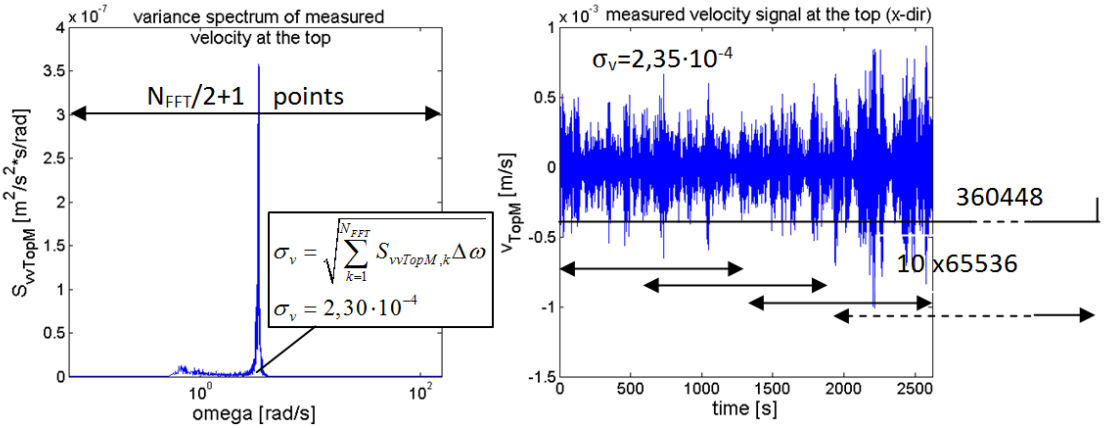

Figure 5 – Variance spectrum of the measured velocity and part of the measured time signal

4.2 Calibration method

In section 2.3 it is explained how the mass and stiffness parameters are calibrated to meet the measured natural frequency (f_n=0.536 Hz). Looking at (41)-(44), the simulated dynamic response depends on 5 unknown factors: a constant load factor C_w and 4 damping parameters, influencing the transfer function. Minimum, maximum and an initial guess values are derived for these parameters. These values (Table 3 and Table 4) are based on theoretical formula's concerning the wind velocity (σ_v, $\overline{v}_0$) and the expected modal damping ratio [14].

	c_D [Ns/m^2]	c_R [Nms/rad]	c_T [Ns/m]	E^*I [Nm^{2}s]
Initial estimate	$1.00\cdot10^4$	$1.00\cdot10^{10}$	$1.00\cdot10^{10}$	$1.00\cdot10^{10}$
minimum	$1.00\cdot10^2$	$1.00\cdot10^4$	$1.00\cdot10^4$	$1.00\cdot10^4$
maximum	$1.00\cdot10^6$	$1.00\cdot10^{15}$	$1.00\cdot10^{15}$	$1.00\cdot10^{15}$

Table 3 – Estimated damping values

	C_w [N^2/m^2]	σ_v [m/s]	C_f [-]	B [m]	ρ_{air} [kg/m^3]	$\overline{v}_0$ [m/s]
Initial estimate	$8.70\cdot10^5$	2.90	1.45	44.3	1.25	4.00
minimum	$2.60\cdot10^4$	1.45	1.00	44.3	1.25	2.00
maximum	$3.80\cdot10^7$	5.80	2.40	44.3	1.25	8.00

Table 4 – Estimated wind load values

The effect of the load is investigated in the case of minimum and maximum damping values according to Table 3. The linear relation between load and response is clearly visible in Figure 6 and Figure 7. For low damping, the absolute effect of the load on the response around the natural frequency is much larger than for frequencies around the quasi static peak (Figure 9). In case of maximum damping values, the effect is vice versa. The quasi static response is the response for a structure that only reacts statically, thus with transfer function at ω=0. The quasi static peak is the result of the peak in the wind spectrum which is visible in Figure 7.

The red line in Figure 8 shows a reasonable fit of the simulated spectrum with the measured spectrum. This fit is obtained by assuming minimum load and damping values and subsequently increasing c_D until it gives a resonance peak comparable to the measurement. As c_D increases, the peak decreases more than proportional and gets wider. The height of the quasi static response doesn't strongly depend on the damping parameters. The same behavior is observed for c_R and E^*I. For c_D=4,4·10^4 Ns/m^2, c_R=2,16·10^{11} Nms/rad and E^*I=2,03·10^{12} Nm^{2}s, a resonance peak comparable to the measurement is found. The influence of c_T is too small to reduce the peak of the resonance peak to match the measured spectrum. This is most probably caused by the large stiffness of k_T. The contribution of this damping term will be neglected and c_T is assumed to have its minimum value.

The question is which combination of load and damping parameters give the best fit with the measured spectrum. The load will mainly influence the height of the quasi static response, and it will also affect the height and width of the resonance peak. The damping parameters will mainly influence the shape of the resonance peak. Because of these three points, it is sufficient to execute a calibration procedure by comparison of the measured spectrum with the simulated spectrum over 6 small ranges of omega (see Figure 9). This reduces calculation time. Comparison over range 1 and 2 provide for proper calibration of the height for the quasi static response. Range 3 and 6 provide for proper calibration of the width of the spectrum, range 4 and 5 take the height of the resonance peak into account.

The response spectrum is simulated for many combinations of different values for C_w, c_D, c_R and E^*I, but c_T=1,0·10^4 Ns/m^2. For every simulation the square of the error between the simulated spectrum and the measured spectrum is calculated for the 6 ranges. The combination with the least square error is the best fitted combination.

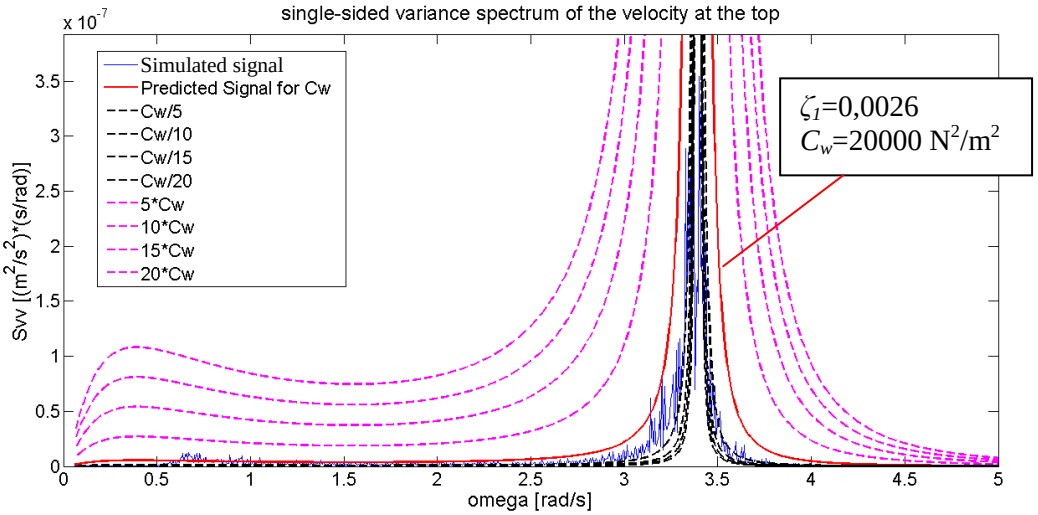

Figure 6 – the effect of load on the simulated response, minimum damping

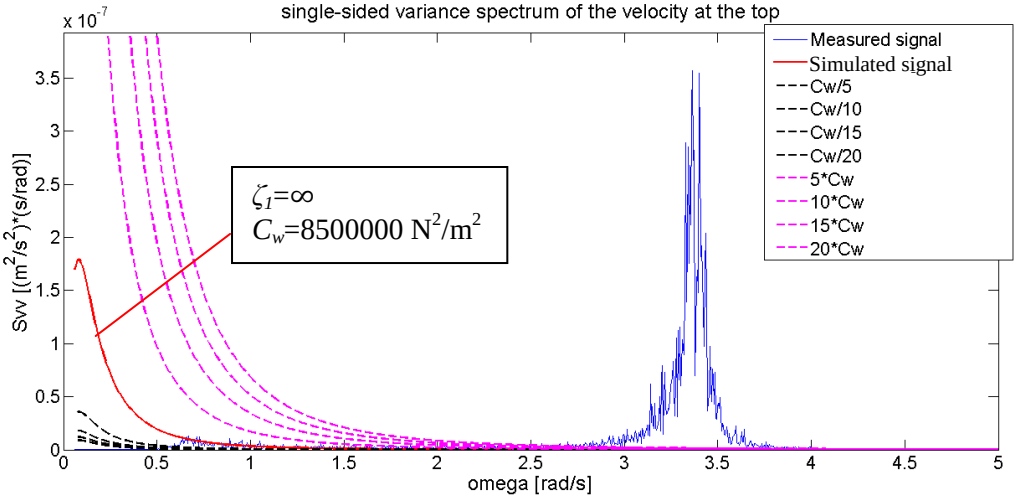

Figure 7 - the effect of the load on the simulated response, maximum damping

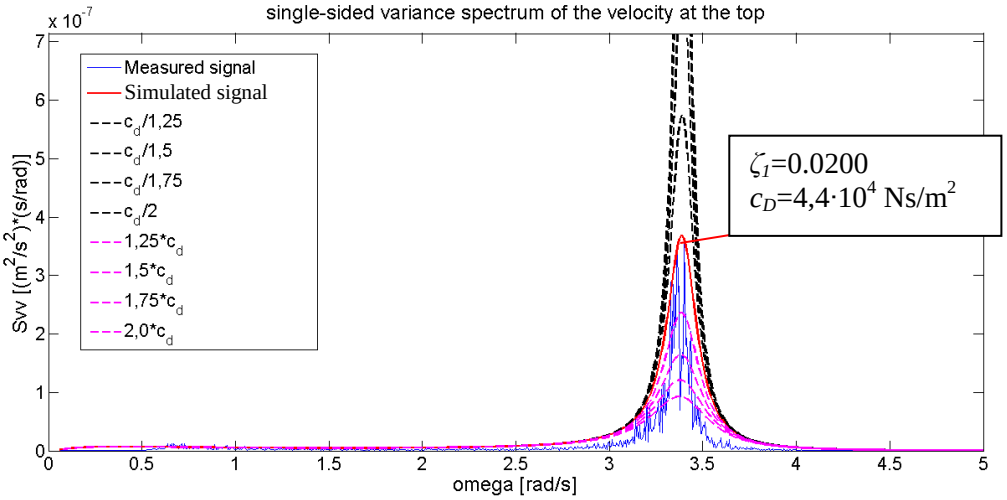

Figure 8 – influence of c_D for minimum C_w , c_R, c_T and E^*I

4.3 Results and conclusion

First the order magnitude is determined by considering the least square error of 3600 combinations of the values indicated in Table 5. An overview of the error, first natural frequency and modal damping ratio of the combinations can be found in Table 6.

	c_D [Ns/m^2]	c_R [Nms/rad]	c_T [Ns/m]	E^*I [Nm^{2}s]	C_w [N^2/m^2]
	$1.00\cdot10^2$	$1.00\cdot10^4$	$1.00\cdot10^4$	$1.00\cdot10^4$	$1.00\cdot10^4$
	$1.00\cdot10^3$	$1.00\cdot10^5$		$1.00\cdot10^5$	$1.00\cdot10^5$
	$1.00\cdot10^4$	$1.00\cdot10^6$		$1.00\cdot10^6$	$1.00\cdot10^6$
	$1.00\cdot10^5$	etc.		etc.	$1.00\cdot10^7$
	$1.00\cdot10^6$	$1.00\cdot10^{15}$		$1.00\cdot10^{15}$	$1.00\cdot10^8$
Number of values	5	12	1	12	5

Table 5 – values used to create combinations

	c_D [Ns/m^2]	c_R [Nms/rad]	c_T [Ns/m]	E^*I [Nm^{2}s]	C_w [N^2/m^2]	Error	ΔError [%]	$\omega_{n,1}$	ζ_1 [%]
1	$1.00\cdot10^{4}$	$1.00\cdot10^{10}$	$1.00\cdot10^{4}$	$1.00\cdot10^{12}$	$1.00\cdot10^{4}$	$1.43\cdot10^{-13}$	0.0	3.394	1.69
2	$1.00\cdot10^{4}$	$1.00\cdot10^{11}$	$1.00\cdot10^{4}$	$1.00\cdot10^{11}$	$1.00\cdot10^{4}$	$1.45\cdot10^{-13}$	1.2	3.394	1.58
3	$1.00\cdot10^{4}$	$1.00\cdot10^{9}$	$1.00\cdot10^{4}$	$1.00\cdot10^{12}$	$1.00\cdot10^{4}$	$1.46\cdot10^{-13}$	2.0	3.394	1.49
4	$1.00\cdot10^{4}$	$1.00\cdot10^{8}$	$1.00\cdot10^{4}$	$1.00\cdot10^{12}$	$1.00\cdot10^{4}$	$1.47\cdot10^{-13}$	3.0	3.394	1.50
5	$1.00\cdot10^{4}$	$1.00\cdot10^{4}$	$1.00\cdot10^{4}$	$1.00\cdot10^{12}$	$1.00\cdot10^{4}$	$1.47\cdot10^{-13}$	3.1	3.394	1.50
6	$1.00\cdot10^{4}$	$1.00\cdot10^{6}$	$1.00\cdot10^{4}$	$1.00\cdot10^{12}$	$1.00\cdot10^{4}$	$1.47\cdot10^{-13}$	3.1	3.394	1.50
7	$1.00\cdot10^{4}$	$1.00\cdot10^{5}$	$1.00\cdot10^{4}$	$1.00\cdot10^{12}$	$1.00\cdot10^{4}$	$1.47\cdot10^{-13}$	3.1	3.394	1.50
8	$1.00\cdot10^{4}$	$1.00\cdot10^{4}$	$1.00\cdot10^{4}$	$1.00\cdot10^{12}$	$1.00\cdot10^{4}$	$1.47\cdot10^{-13}$	3.1	3.394	1.50
9	$1.00\cdot10^{4}$	$1.00\cdot10^{11}$	$1.00\cdot10^{4}$	$1.00\cdot10^{10}$	$1.00\cdot10^{4}$	$1.58\cdot10^{-13}$	11	3.399	1.38
10	$1.00\cdot10^{4}$	$1.00\cdot10^{11}$	$1.00\cdot10^{4}$	$1.00\cdot10^{9}$	$1.00\cdot10^{4}$	$1.61\cdot10^{-13}$	13	3.399	1.39
11	$1.00\cdot10^{4}$	$1.00\cdot10^{11}$	$1.00\cdot10^{4}$	$1.00\cdot10^{8}$	$1.00\cdot10^{4}$	$1.62\cdot10^{-13}$	13	3.399	1.39
12	$1.00\cdot10^{4}$	$1.00\cdot10^{11}$	$1.00\cdot10^{4}$	$1.00\cdot10^{7}$	$1.00\cdot10^{4}$	$1.62\cdot10^{-13}$	13	3.399	1.39
13	$1.00\cdot10^{4}$	$1.00\cdot10^{11}$	$1.00\cdot10^{4}$	$1.00\cdot10^{6}$	$1.00\cdot10^{4}$	$1.62\cdot10^{-13}$	13	3.399	1.39
14	$1.00\cdot10^{4}$	$1.00\cdot10^{11}$	$1.00\cdot10^{4}$	$1.00\cdot10^{5}$	$1.00\cdot10^{4}$	$1.62\cdot10^{-13}$	13	3.399	1.39
15	$1.00\cdot10^{4}$	$1.00\cdot10^{11}$	$1.00\cdot10^{4}$	$1.00\cdot10^{4}$	$1.00\cdot10^{4}$	$1.62\cdot10^{-13}$	13	3.399	1.39
16	$1.00\cdot10^{2}$	$1.00\cdot10^{11}$	$1.00\cdot10^{4}$	$1.00\cdot10^{12}$	$1.00\cdot10^{4}$	$2.68\cdot10^{-13}$	88	3.394	2.02
17	$1.00\cdot10^{3}$	$1.00\cdot10^{11}$	$1.00\cdot10^{4}$	$1.00\cdot10^{12}$	$1.00\cdot10^{4}$	$2.84\cdot10^{-13}$	99	3.394	1.98

Table 6 – overview of combinations with the least error

When looking at the combinations with the lowest error it can be concluded that the load will have order of magnitude 10^4. The other combinations (1-17) with low error also show some interesting aspects because three ranges can be distinguished. In each range, one of the three relevant damping parameters (c_D, c_R and E^*I) can vary a lot without influencing the error significantly. Consider for example c_R for combination 1-8. The shape of the resonance peak is governed by the damping contribution of the other two damping sources (c_D and E^*I). The range in which c_R can vary freely, are values below the order of magnitude for the respective parameter (except for combination 2, where E^*I has a lower value, such that c_R can be higher). It can be concluded that the order of magnitude for the parameters that give the least error are:

c_D [Ns/m^2]	c_R [Nms/rad]	c_T [Ns/m]	E^*I [Nm^{2}s]	C_w [N^2/m^2]
$1.00\cdot10^{4}$	$1.00\cdot10^{11}$	-	$1.00\cdot10^{12}$	$1.00\cdot10^{4}$

Table 7 – order of magnitude for the parameters to obtain the best fit

In order to find an even better fit, the same procedure is repeated for values around the found order of magnitude for c_D, c_R, E^*I and C_w. For each parameter 19 values have been assumed, ranging from 10% to 190% of the found order of magnitude. For example considering c_D, these values are: $1\cdot10^3$, $2\cdot10^3$, $3\cdot10^3$, … $8\cdot10^4$, $9\cdot10^4$. Combinations with even smaller errors are found, an example of such fit can be found in Figure 9. However combinations with different damping values have comparable small errors. No unique solution is found and the relative contribution of c_D, c_R and E^*I can't be determined because the parameters influence the resonance peak in the same way. It can only be concluded that the damping parameters have a value between 10% and 190% of the values in Table 7. For the load parameters, C_w it is possible to give a more accurate estimation of the magnitude because the fits with the least square error all had a value of $1\cdot10^4$ or $2\cdot10^4$ N^2/m^2.

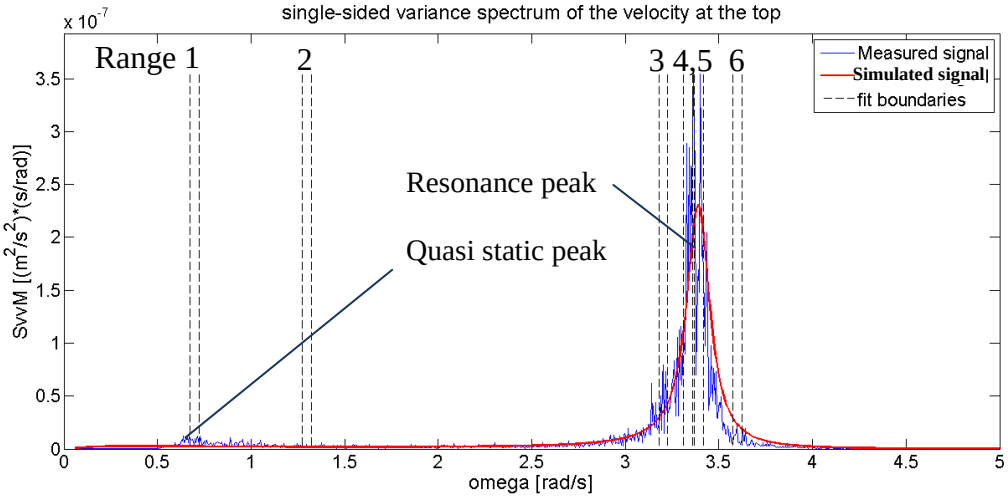

Figure 9 – simulated response for well fitted combination

5 CONCLUSION

In this paper a building model is introduced to investigate the possibilities on identifying the relative damping contribution of different building parts. This is done by a numerical calibration of the simulated response to the measured response (Figure 9). By making use of the design calculations and the measured dynamic response of the building, the mass and stiffness parameters of the building were calibrated by comparison of the simulated and actual natural frequency of the first mode. Since no information about the local wind loading conditions was available, the magnitude of the variance of the wind load at time of measurement was unknown. Theoretical assumptions made it possible to define the shape of the wind loading spectrum along the height of the building, which can be multiplied with an unknown wind loading factor C_w to obtain the wind loading spectrum. With the transfer function derived from the model, it was possible to simulate the response at the top of the building. The transfer function depends on the a priori unknown damping parameters: c_D, c_R, c_T and E^*I. The response spectrum is simulated for many combinations of different values for these parameters.

Best fit values for C_w, c_D, c_R, c_T and E^*I are found from the combination that resulted in the least square error between the simulated and measured response spectrum at the quasi static and resonance response. In conclusion it is possible to give a quite accurate estimation of the load factor C_w, the effect of c_T can be neglected, but it is not possible to identify the relative contribution of the other three damping parameters. The latter is caused by the fact the three parameters influence the shape of the resonance peak in the same manner. Many different combinations of values for these parameters lead to a fit with (almost) equal error. From this research it can be concluded that only the total damping of the first mode which has been identified from the measured response at the top only, is insufficient to determine the relative contribution of the four damping contributions as modeled.

6 FUTURE DEVELOPMENTS

Ongoing research focuses on the development of a physically more correct damping model together with an improvement/extension of the current measurement methods. This should result in a better identification of the effect of different damping mechanisms on the response spectrum and more data to be available for calibration. Eventually this should allow one to identify the damping contribution of the different building parts.

Current investigation explores the possibilities of a building model in which the main lateral stabilizing structural system (the core) and the non-stabilizing part (floors, beams etc.) are represented by an Euler-Bernoulli beam and a shear beam, coupled together. This model should allow us to better implement the damping mechanisms in, and the interaction between, these parts. Furthermore the usability and accuracy of implementation of theoretical formulae for the different damping mechanism is investigated. Another research topic is the implementation of other damping models than the viscous behavior. Literature indicates internal material damping is better described by a mathematical description based on frequency independent hysteresis damping. In addition, it is more realistic to implement friction elements to model the energy loss at the interfaces between elements [6; 14]. The characteristic effects of these different damping models on the simulated response should be investigated and compared to the actual response.

By measurement of the building response at different levels, it should be possible to identify the total damping of the second mode [15], this makes it possible to use two instead of one resonance peak to calibrate the model. It is investigated if this allows us to uniquely determine the values of the different damping parameters.

It is also planned to monitor the rotation at the building's base simultaneously with the lateral displacement to possible identify the contribution of the energy loss at the interface with the ground.

REFERENCES

[1] ISO6897: Guidelines for the evaluation of the response of occupants of fixed structures. (1986).

[2] Koten, H. van. (1977). CUR rapport 75, demping van bouwconstructies: TNO.

[3] NNI. (2005). NEN-EN 1991-1-4: general actions - wind actions. Delft.

[4] Berg, R.L.J. van den. (2012). *Investigation of damping in high-rise buildings: Identification and prediction in the serviceability limit state for wind-induced vibrations (MSc-thesis).* Faculty of Civil engineering and Geosciences, Delft.

[5] Jeary, A.P. (1986). Damping in tall buildings - a mechanism and a predictor. *Earthquake engineering and structural dynamics, 14*, 733-750.

[6] Lagomarsino, S. (1993). Forecast models for damping and vibration periods of buildings. *Journal of Wind Engineering and Industrial Aerodynamics, 48*, 221-239.

[7] Satake, N., Suda, K., Arakawa, T., Sasaki, A., & Tamura, Y. (2003). Damping evaluation using full-scale data of buildings in Japan. *Journal of structural engineering*, 470-477.

[8] Li, Q.S., & Wu, J.R. (2007). Time-frequency analysis of typhoon effects on a 79-storey tall building. *Journal of Wind Engineering and Industrial Aerodynamics, 95*, 1648-1666.

[9] Bashor, R., Bobby, S., Kijewski-Correa, T., & Kareem, A. (2012). Full-scale performance evaluation of tall buildings under wind. *Journal of Wind Engineering and Industrial Aerodynamics, 104-106*, 88-97.

[10] Simone, A. (2009). *An introduction to the analysis of slender structures, lecture notes CT4190*. Delft: Faculty of Civil Engineering and Geosciences.

[11] Vrouwenvelder, A.C.W.M. (2004). *Random Vibrations, Lecture notes CT5145*: Faculty of Civil Engineering and Geosciences.

[12] Oosterhout, G.P.C. van. (1996). *Thesis: Wind-induced dynamic behaviour of tall buildings.* TUDelft, Delft.

[13] Welch, P.D. (1967). The use of Fast Fourier Transform for the estimation of power spectra: a method based on time avergaging over short, modified periodograms. *IEEE Trans. Audio and electroacoust, AU-15*, 70-73.
[14] Lazan, B. (1968). *Damping of materials and members in structural mechanics*. London: Pergamon Press.
[15] Guo, Y.L., Kareem, A., Ni, Y.Q., & Liao, W.Y. (2012). Performance evaluation of Canton Tower under wunds based on full-scale data. *Journal of Wind Engineering and Industrial Aerodynamics, 104-106*, 116-128.